Supplementary for ‘Carbonation-front prediction and practical identifiability of transport-reaction parameters in solid-waste backfill materials using inverse modeling”

Supplementary Note S1. Evidence-ranked protocol

The formal ranking matrix $\mathcal{D}_{\text{rank}}$ contains paired carbonation-depth and UCS observations. Uptake and extent-proxy observations are reserved for consistency checks unless a source provides the same train–validation–test structure as the formal depth–UCS matrix.

The pre-specified stratified split contained 28 training observations, 8 validation observations, and 8 test observations. Each split preserved the four initial-carbonation-age groups: 7 training, 2 validation, and 2 test observations per group. All formal candidate models used the same split manifest and random seeds within each evaluation protocol. The one-dimensional domain length was $L = 100$ mm, and time was represented in days with neural-network inputs scaled by the 31 d observation duration. The effective transport–reaction parameters are therefore reported on the inverse-model scale used by the nondimensionalized neural inputs.

Supplementary Note S2. Full inverse-model operators

The group-conditioned effective parameters used in the diagnostic hierarchy were

$$\log D_g = \log D_0 + \delta_D(g), \tag{1}$$

$$\log k_g = \log k_0 + \delta_k(g), \tag{2}$$

$$\nu_g = \nu_0 + \delta_\nu(g), \tag{3}$$

with deviation penalty

$$\mathcal{L}_{\text{group}} = \sum_g [\delta_D(g)^2 + \delta_k(g)^2 + \delta_\nu(g)^2]. \tag{4}$$

The initial-age group is treated as an effective covariate rather than as a resolved hydration, moisture, or pore-structure state. Accordingly, all groups share the normalized initial latent-field conditions $c(x, 0; g) = 0$ and $b(x, 0; g) = 1$, while group effects enter through the age input to the neural field and, when enabled, through grouped effective parameters.

The UCS response operator used in the pre-specified PINN evaluation was a supervised multilayer-perceptron head,

$$\widehat{s}(t, g) = f_s\left(\widehat{d}(t, g)/L, g/\max(g)\right), \tag{5}$$

with two hidden layers and hidden width 24. It was trained jointly with the latent-field network when UCS supervision was retained. This head is an auxiliary observation model and is not a PDE state or a constitutive strength law. For multi-source diagnostics, the mean latent carbonation degree was

$$\bar{\alpha}(t, g) = \frac{1}{L}\int_0^L \alpha(x, t; g)\,\mathrm{d}x. \tag{6}$$

The uptake and extent-proxy consistency operators were

$$\widehat{U}(t,g) = f_U[\bar{\alpha}(t,g), g, \xi_U], \tag{7}$$

and

$$\widehat{A}(t,g) = f_A\left(\sigma\left[\frac{\bar{\alpha}(t,g) - \alpha_{\mathrm{ph}}}{\tau_A}\right], g, \xi_A\right), \tag{8}$$

where ξ_U and ξ_A denote study-specific covariates when reported. If a spatially resolved area-ratio label were available, a stricter operator would be

$$\frac{1}{L}\int_0^L \sigma\left[\frac{\alpha(x,t;g) - \alpha_{\mathrm{ph}}}{\tau_A}\right] \mathrm{d}x. \tag{9}$$

These uptake and extent operators are consistency mappings only. They do not impose carbon mass balance, mineral-product stoichiometry, or sequestration-capacity accounting.

The multi-source observation loss was

$$\mathcal{L}_{\mathrm{obs}} = \sum_{m \in Q} \{\exp(-\eta_m)\mathcal{J}_m + \eta_m\}, \tag{10}$$

and the diagnostic objective was

$$\begin{aligned}\mathcal{L}_{\mathrm{multi}} = \mathcal{L}_{\mathrm{obs}} &+ \lambda_{\mathrm{pde}}\{\exp(-\eta_{\mathrm{pde}})\mathcal{L}_{\mathrm{pde}} + \eta_{\mathrm{pde}}\} \\ &+ \lambda_{\mathrm{bc}}\mathcal{L}_{\mathrm{bc}} + \lambda_{\mathrm{ic}}\mathcal{L}_{\mathrm{ic}} + \lambda_{\mathrm{group}}\mathcal{L}_{\mathrm{group}} + \lambda_{\mathrm{mono}}\mathcal{L}_{\mathrm{mono}}.\end{aligned} \tag{11}$$

The PDE residuals at collocation points were

$$R_c = \frac{\partial c}{\partial t} - \frac{\partial}{\partial x}\left[D(\alpha)\frac{\partial c}{\partial x}\right] + kcb, \tag{12}$$

$$R_b = \frac{\partial b}{\partial t} + \nu kcb, \tag{13}$$

with mean residual magnitude

$$\overline{R}_{\mathrm{pde}} = \frac{1}{N_c}\sum_{j=1}^{N_c}\left[R_c(x_j,t_j,g_j)^2 + R_b(x_j,t_j,g_j)^2\right]. \tag{14}$$

A monotonicity diagnostic was evaluated by

$$V_x = \frac{1}{N_c}\sum_j \max(0, \partial_x \alpha_j)^2, \tag{15}$$

$$V_t = \frac{1}{N_c}\sum_j \max(0, -\partial_t \alpha_j)^2, \tag{16}$$

$$\mathcal{L}_{\mathrm{mono}} = V_x + V_t. \tag{17}$$

Supplementary Note S3. Empirical front baselines

The empirical baseline ladder used the same split protocols as the mechanistic models. The grouped square-root law was

$$\widehat{d}(t, g) = a_g \sqrt{t} + b_g, \tag{18}$$

the grouped power law was

$$\widehat{d}(t, g) = a_g t^{p_g} + b_g, \tag{19}$$

and the grouped Weibull front law was

$$\widehat{d}(t, g) = d_{\infty,g} \left[1 - \exp\left[-\left(\frac{t}{\lambda_g} \right)^{m_g} \right] \right] + b_g. \tag{20}$$

The monotone spline baseline was

$$\widehat{d}(t, g) = b_g + \sum_{\ell=1}^{K} \theta_{\ell,g} B_\ell(t), \tag{21}$$

with monotonicity penalty

$$\mathcal{L}_{\text{spline}} = \sum_i [\widehat{d}(t_i, g_i) - d_i]^2 + \lambda_{\text{mono},d} \sum_j \max\left(0, -\frac{\partial \widehat{d}(t_j, g_j)}{\partial t} \right)^2. \tag{22}$$

These baselines are only predictive front regressors and do not define latent carbonation fields.

Supplementary Note S4. Repeated split, PDE-weight, and threshold diagnostics

For repeated split evaluation, the split-specific error for model m on split b was

$$\text{RMSE}_{d,bm} = \left[\frac{1}{N_b} \sum_{i \in \mathcal{T}_b} (\widehat{d}_{im} - d_i)^2 \right]^{1/2}, \tag{23}$$

with analogous definitions for MAE and UCS metrics. The full PDE-weight sweep used

$$\lambda_{\text{pde}} \in \{0, 10^{-4}, 10^{-3}, 10^{-2}, 10^{-1}, 1, 10, 100\}. \tag{24}$$

Nested threshold validation used the candidate set

$$\mathcal{A} = \{0.30, 0.35, 0.40, 0.45, 0.50, 0.55, 0.60, 0.65, 0.70\}, \tag{25}$$

and selected

$$\alpha^*_{\text{ph}} = \arg\min_{\alpha \in \mathcal{A}} \text{RMSE}_{d,\text{val}}(\alpha). \tag{26}$$

Supplementary Note S5. Practical-identifiability diagnostics

For $\theta = (\log D_0, \log k, \nu, \gamma)$, the profile loss for parameter θ_j was

$$\mathcal{P}_j(z) = \min_{\theta_{-j},\phi} \mathcal{L}_{\mathrm{val}}(\theta_j = z, \theta_{-j}, \phi), \tag{27}$$

with normalized increment

$$\Delta\mathcal{P}_j(z) = \mathcal{P}_j(z) - \min_z \mathcal{P}_j(z). \tag{28}$$

The profile flatness score was

$$F_j = \frac{\max_z \Delta\mathcal{P}_j(z) - \min_z \Delta\mathcal{P}_j(z)}{|\min_z \mathcal{P}_j(z)| + \epsilon}. \tag{29}$$

The local sensitivity matrix was

$$S_{ij} = \frac{\partial y_i}{\partial \theta_j}, \tag{30}$$

or, when automatic differentiation was not used for the diagnostic,

$$S_{ij} \approx \frac{y_i(\theta_j + h_j) - y_i(\theta_j - h_j)}{2h_j}. \tag{31}$$

The weighted Fisher matrix and approximate covariance/correlation diagnostics were

$$F = S^T W S, \qquad C = F^+, \qquad \rho_{ij} = \frac{C_{ij}}{\sqrt{C_{ii}C_{jj}}}, \tag{32}$$

where F^+ is the Moore-Penrose pseudo-inverse used for ill-conditioned matrices.

Supplementary Note S6. Consistency checks using additional literature data

The additional literature data were used to examine observation-level compatibility with related strength, uptake, and carbonation-extent trends. They were not used for formal model ranking, parameter transfer, or external validation. The formal ranking reported in the main manuscript remains based on the paired carbonation-depth and UCS matrix from Fang et al. [1].

S6.1. Auxiliary strength reconstruction under high-CO_2 curing

The high-CO_2 curing measurements reported by Fang et al. [2] do not provide the same paired depth–UCS structure as the formal model-ranking dataset. They therefore support a narrower assessment of auxiliary strength trends under approximate front constraints. The UCS reconstruction yielded a mean MAE of 1.117 MPa, RMSE of 1.276 MPa, and $R^2 = 0.817$, while the predicted front remained inside the weak constraint envelope. This result supports strength-response compatibility within this additional dataset, but does not imply transferability of the effective transport–reaction parameters.

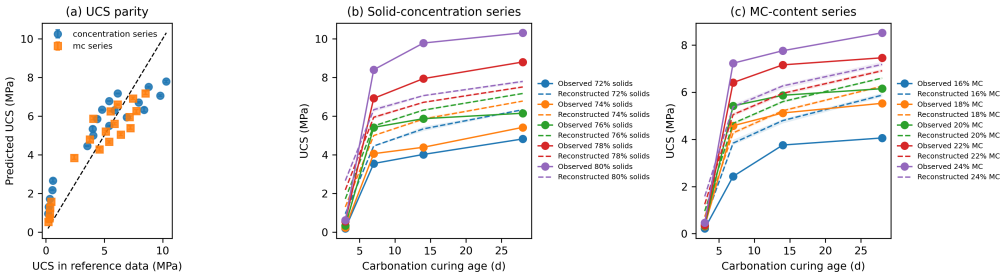


Figure S1: In-sample auxiliary UCS reconstruction for the high-CO_2 curing measurements reported by Fang et al. [2]. MC denotes magnesium-coal-slag backfill material content. The panels assess whether strength trends can be represented without promoting UCS to a PDE state.

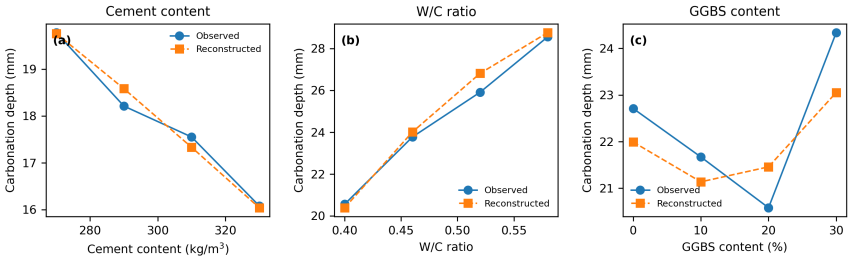


Figure S2: In-sample carbonation-depth reconstruction for the mixture-variable measurements reported by Cheng et al. [3]. These panels provide related-system consistency checks and are not a held-out transfer test of the selected model.

S6.2. Depth–UCS reconstruction in mixture-variable measurements

The mixture-variable measurements reported by Cheng et al. [3] provide both carbonation-depth and UCS labels in a related material system, making them the most informative additional reconstruction case. The constrained formulation reconstructed the paired responses closely in sample, with depth MAE 0.458 mm, depth RMSE 0.587 mm, depth R^2 = 0.989, UCS MAE 1.860 MPa, UCS RMSE 2.183 MPa, and UCS R^2 = 0.897. These results indicate representational compatibility in a related system. Because the reconstruction was in sample, it remains a consistency check rather than a held-out transfer test. The GGBS-content subset shows larger deviations than the other mixture sweeps, suggesting that mixture-dependent chemistry is not fully represented by the present group-conditioned formulation.

S6.3. Carbonation-curing strength and uptake consistency

The carbonation-curing measurements reported by Fang et al. [4] do not provide a systematic front-depth table suitable for formal depth ranking. They instead support a consistency analysis between reconstructed UCS trends and independently reported carbon uptake. The UCS reconstruction yielded MAE 0.378 MPa, RMSE 0.596 MPa, and R^2 = 0.958. The uptake consistency score was 1.0 and the pairwise strength–uptake trend score was 0.9. This result provides auxiliary consistency evidence for the strength-response component, but it does not identify transport parameters.

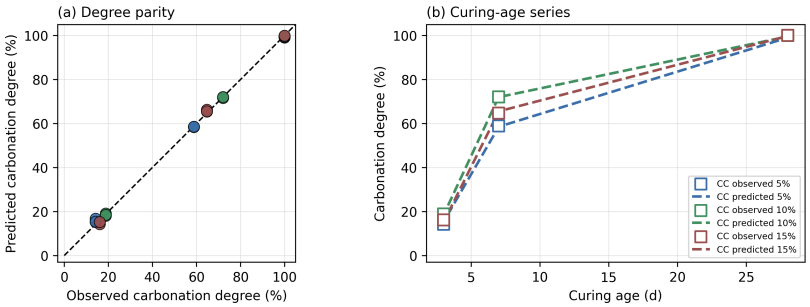


Figure S3: In-sample extent-proxy reconstruction using carbonation-degree area-ratio observations for the low-CO_2 curing observations reported by Chen et al. [5]. The trends are interpreted as extent consistency rather than front-depth validation.

S6.4. Carbonation-extent consistency based on area-ratio observations

The observations reported by Chen et al. [5] provide carbonation degree as an area-ratio or extent-type label rather than as a systematic one-dimensional front depth. The analysis therefore uses the reported carbonation degree as an extent proxy. The carbonation-degree reconstruction has RMSE 0.855 percentage points, and the uptake consistency score is 0.867. This result is qualitatively consistent with a link between carbonation extent, uptake, and reported material evolution, while preserving the distinction between extent proxies and true front-depth observations.

References

[1] Z. Fang, L. Liu, W. He, K. Han, H. Lan, Y. Gao, W. Sun, Z. Han, L. Xia, P. Yang, Strength characteristics and carbonation depth evolution of modified magnesium slag based solid waste storage backfill materials, Journal of Environmental Chemical Engineering 12 (2) (2024) 111975. doi:10.1016/j.jece.2024.111975.

[2] Z. Fang, L. Liu, X. Zhang, K. Han, J. Wang, M. Zhu, W. Sun, W. He, Y. Gao, Carbonation curing of modified magnesium-coal based solid waste backfill material for co2 sequestration, Process Safety and Environmental Protection 180 (2023) 778–788. doi:10.1016/j.psep.2023.10.049.

[3] F. Cheng, Q.-H. Wang, Experimental study on the carbonation performance of cemented tailings artificial pillars, Construction and Building Materials 494 (2025) 143284. doi:10.1016/j.conbuildmat.2025.143284.

[4] Z. Fang, Y. Gao, W. He, M. Zhu, L. Xia, P. Yang, D. Liu, J. He, Carbonation curing of magnesium-coal slag solid waste backfill material: Study on properties of flow, mechanics and carbon sequestration, Case Studies in Construction Materials 20 (2024) e03204. doi:10.1016/j.cscm.2024.e03204.

[5] Q. Chen, L. Zhu, Y. Wang, J. Chen, C. Qi, The carbon uptake and mechanical property of cemented paste backfill carbonation curing for low concentration of CO_2, Science of the Total Environment 852 (2022) 158516. doi:10.1016/j.scitotenv.2022.158516.